DOI: 10.1002/ejic.201000088

# A Supramolecular Derivative of a Nanoporous Molybdenum Oxide Based Inorganic Keplerate with Self-Defocusing Nonlinear Optical Properties

**Lijuan Zhang,[a] Yunshan Zhou,*[a] and Ruixue Han[a]**

**Keywords:** Structure elucidation / Organic–inorganic hybrid composites / Nonlinear optics / Keplerates

A new derivative of the highly charged inorganic Keplerate of the type {pentagon}$_{12}${linker}$_{30}$ ≡ {(Mo)$Mo_5O_{21}$-$(H_2O)_6$}$_{12}${$Mo_2O_4(SO_4)$}$_{30}$ with the formula $(NH_4)_{28}(NH_2$-$CHNH_2)_6Gd_3$[{$(NH_2CHNH_2)_{20}$ + $Gd_3$ + $(H_2O)_{50}$} ⊂ {($Mo^{VI}$)-$Mo^{VI}{}_5O_{21}(H_2O)_6$}$_{12}$ {$Mo^{V}{}_2O_4(SO_4)$}$_{30}$]·ca.250$H_2O$ was isolated and characterized by elemental analysis, IR and UV/Vis spectroscopy, single-crystal X-ray analysis, and magnetic susceptibility measurements. Three $Gd^{3+}$ ions are found inside the internal cavity of the capsule. The coordination sphere of each $Gd^{3+}$ ion is completed by the oxygen atoms of $SO_4$ groups that act as bidentate ligands to a {$Mo_2$} linker and by the oxygen atoms of the encapsulated new two-shell underoccupied [{$H_2O$}$_{60+20}$ + {$H_2O$}$_{20}$] water cluster that acts as polydentate ligand. Twenty $HC(NH_2)_2^+$ cations interact with the twenty {$Mo_9O_9$} pores through hydrogen bonds between the O and H atoms of the two $NH_2$ groups, which demonstrates a surface supramolecular chemistry. Of importance, a third-order nonlinear optical investigation, using the Z-scan technique, shows for the first time that the derivative demonstrates a strong self-defocusing third-order nonlinear optical effect with large third-order nonlinear optical susceptibility. This observation implies that these unique inorganic Keplerates and their derivatives might find applications in nonlinear optical materials science.

## Introduction

Polyoxometalates (POMs) formed by the early transition metals, incorporating nearly every element of the periodic table, constitute a vast class of inorganic cluster systems characterized by an intriguing variety of architectures and topologies, and find applications in catalysis, biology, magnetism, nanoscience, optics, and medicine.[1]

It is known that increasing the size and the complexity of POMs can generate multifunctionality of interest to materials science.[2] In an effort to design well-defined nanoscaled giant polyoxometalates from simple inorganic building blocks, the nanosized inorganic super fullerenes of the type {pentagon}$_{12}${linker}$_{30}$ ≡ {(Mo)$Mo_5O_{21}(H_2O)_6$}$_{12}$-{$Mo_2O_4$(ligand)}$_{30}$ were first synthesized by Müller's group.[3a] The giant polyoxometalate cluster possesses unique features including 20 {$Mo_9O_9$} type pores with crown-ether like functionality that can be opened and shut with noncovalently bonded substrates such as guanidinium cations[3b] and 20 channels directly connected with the pores. The size and charge of the capsule can be tuned by changing the linkers, and the shell functionality of the inner cavity can be tuned by changing the ligands. Many properties and applications of these clusters have been found and developed[3] such as modeling passive cation transport through membranes,[3c] encapsulation and nanoseparation chemistry,[3d] generating structures of confined water,[3e] coordination chemistry under confined conditions,[3f] as well as modeling ligand exchange at oxide mineral surfaces.[3g,3h]

Besides the interesting properties and applications noted above, the inorganic super fullerenes of the type {(Mo)-$Mo_5O_{21}(H_2O)_6$}$_{12}${$Mo_2O_4$(ligand)}$_{30}$ comprise 72 $Mo^{VI}$ atoms with empty 4d orbitals and 60 $Mo^{V}$ atoms, and are categorized as type I within the Robin–Day classification for mixed-valence compounds.[4] This characteristic could be important to materials science as it may result in extensive polarization of charge when the molecules are exposed to electromagnetic radiation, which would bring about a good nonlinear optical (NLO) response.

Herein we report the preparation, characterization, magnetic and self-defocusing third-order nonlinear optical properties of a new derivative of the highly charged inorganic Keplerate[3j] with the formula $(NH_4)_{28}$-$(NH_2CHNH_2)_6Gd_3$[{$(NH_2CHNH_2)_{20}$ + $Gd_3$ + $(H_2O)_{50}$} ⊂ {($Mo^{VI}$)$Mo^{VI}{}_5O_{21}(H_2O)_6$}$_{12}${$Mo^{V}{}_2O_4(SO_4)$}$_{30}$]·ca. 250$H_2O$ (**1**).

## Results and Discussion

### Structure Description of 1

According to the single-crystal X-ray structure analysis, capsule **1a** shows the characteristic spherical skeleton {pentagon}$_{12}${linker}$_{30}$ ≡ {(Mo)$Mo_5O_{21}(H_2O)_6$}$_{12}${$Mo_2O_4$-

[a] State Key Laboratory of Chemical Resource Engineering, Institute of Science, Beijing University of Chemical Technology, Beijing 100029, P. R. China
Fax: +86-10-64414640
E-mail: zhouyun0734@sina.com.cn
zhouys@mail.buct.edu.cn

Supporting information for this article is available on the WWW under http://dx.doi.org/10.1002/ejic.201000088.

  

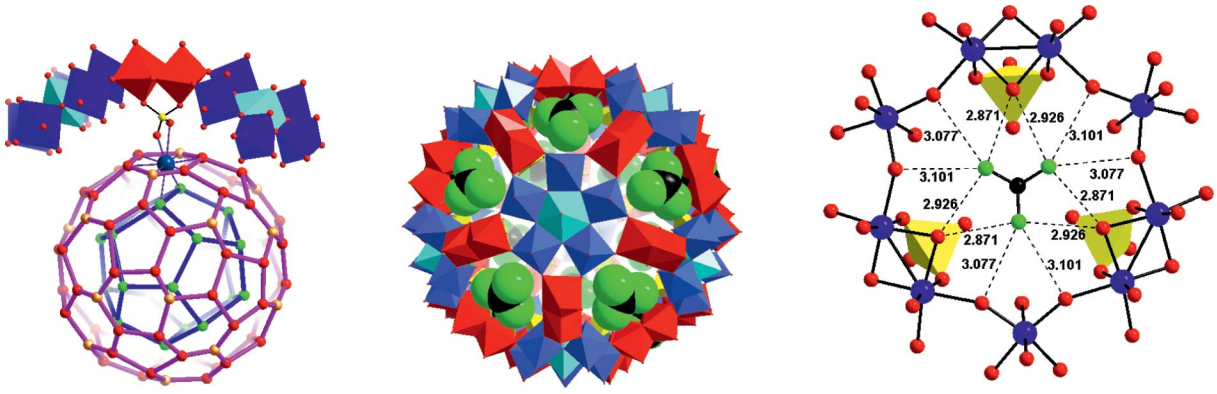


Figure 1. (a) Part of the structure of **1a**: The underoccupied 30 $Gd^{3+}$ ion positions inside the capsule form, together with the $\{H_2O\}_{60+20}$ cluster shell positions [the $\{H_2O\}_{60}$ is shown in red and the $\{H_2O\}_{20}$ in pink] and the inner $\{H_2O\}_{20}$ cluster shell positions (in green), a new type of spherical cluster shell (Gd dark blue, O red and pink). A fragment of the metal oxide skeleton of the capsule is also shown (polyhedral representation; Mo blue or cyan, O red) symmetrically coordinated to one sulfate group (ball-and stick representation; S yellow). (b) Space filling representation of the encapsulated formamidinium cations (disordered in agreement with the $C_3$ axes passing through the pores; C black, N green) plugging the 20 $\{Mo_9O_9\}$ type pores on the surface of the molybdenum oxide skeleton shown in polyhedral representation. (c) The interatomic distances for the $\{Mo_9O_9\}$ rings in **1a** reflecting the interaction between the receptors and substrates. These are comparable with those known from related single host–guest systems with classical macrocycles.

$(NH_4)_{28}(NH_2CHNH_2)_6Gd_3[\{(NH_2CHNH_2)_{20} + Gd_3 + (H_2O)_{50}\} \subset \{(Mo^{VI})Mo^{VI}_5O_{21}(H_2O)_6\}_{12}\{Mo^{V}_2O_4(SO_4)\}_{30}]\cdot ca.250H_2O \equiv (NH_4)_{28}(NH_2CHNH_2)_6Gd_3\cdot$**1a**$\cdot ca.250H_2O \equiv$ **1**

$(NH_4)_{72-n}[\{(H_2O)_{81-n} + (NH_4)_n\}\{(Mo^{VI})Mo^{VI}_5O_{21}(H_2O)_6\}_{12}\{Mo^{V}_2O_4(SO_4)\}_{30}]\cdot ca.200H_2O \equiv (NH_4)_{72-n}\cdot$**2a**$\cdot ca.200H_2O \equiv$ **2**

$(NH_4)_{25}(NH_2CHNH_2)_6Pr_3[\{(NH_2CHNH_2)_{20} + Pr_4 + (H_2O)_{40}\} \subset \{(Mo^{VI})Mo^{VI}_5O_{21}(H_2O)_6\}_{12}\{Mo^{V}_2O_4(SO_4)\}_{30}]\cdot ca.240H_2O \equiv (NH_4)_{25}(NH_2CHNH_2)_6Pr_3\cdot$**3a**$\cdot ca.\ 240H_2O$ (**3**)

$(NH_4)_{27}[Pr(H_2O)_9]_{10}[(Pr_5) \subset \{(Mo^{VI})Mo^{VI}_5O_{21}(H_2O)_6\}_{12}\{Mo^{V}_2O_4\ (SO_4)\}_{30}]\cdot ca.\ [180H_2O + 12Cl^- + 3Pr^{3+} + 3NH_4^+] \equiv (NH_4)_{27}[Pr(H_2O)_9]_{10}\cdot$**4a**$\cdot$[cocrystallized components] (**4**)

$(SO_4)\}_{30}$,[3e] built up from 12 $\{Mo_6\}$ fragments of the type $\{(Mo)Mo_5\}$, linked by 30 $\{Mo_2\}$ fragments of the type $\{Mo_2O_4(SO_4)\}_{30}$ with bidentate sulfate ligands as stabilizers. This construction principle leads to capsules with 20 $\{Mo_9O_9\}$ type pores (Figure 1). The high symmetry of the anion is also proven by the presence of just a few lines in the Raman spectrum, which is quite similar to that of compound **2** (Figure S1). All of the O atoms of the 132 Mo–$O_{term}$ groups lie on the outer sphere surface, and correspondingly the *trans*-positioned $H_2O$ ligands of the 72 $Mo^{VI}$ centers point to the center of the sphere (Figure 1).

Of further interest is the interior of the cavity of **1a**, which hosts an interesting new water cluster (Figure 1a) consisting of two shells: an outer $\{H_2O\}_{60+20}$ shell and an inner $\{H_2O\}_{20}$ shell, a situation that differs from those found in compounds **2**,[3e] **3**,[3f] and **4**.[3i] The cavity of **2a** hosts a fully occupied two-shell water $\{H_2O\}_{80}$ cluster, the outer shell is a $\{H_2O\}_{60}$ cluster forming a strongly distorted rhombicosidodecahedron and the inner is a $\{H_2O\}_{20}$ cluster forming a dodecahedron. The water cluster in **3a** is similar to that in **2a**, but it is half occupied. In **4a**, the encapsulated water molecules form a partially occupied $\{H_2O\}_{60+20}$ shell, formally described as $\{H_2O\}_{60}$ + $\{H_2O\}_{20}$, which is different from that in **2a**. Of interest in **1a** is that the encapsulated water molecules form a small inner underoccupied $\{H_2O\}_{20}$ shell that is similar to that found in **3a** and an underoccupied outer $\{H_2O\}_{60+20}$ shell (i.e., a distorted rhombicosidodecahedron + a dodecahedron with the O atoms located on the $C_3$ axis) similar to that found in **4a**. The distances from the capsule center to each vertex of the inner dodecahedron range from 4.921 to 4.980 Å with the O···O distances in the range of 3.368–3.717 Å (average 3.533 Å), whereas the distances from the capsule center to each vertex (i.e., the O atoms located on the $C_3$ axis) of the outer dodecahedron composing the $\{H_2O\}_{60+20}$ shell range from 6.984 to 7.378 Å (average 7.257 Å) with the O···O distances in the range of 1.963 to 3.025 Å (Table 1). The abnormality of some of the O···O distances is rationally attributed to low occupancy/disorder of the water molecules.

Each of the three encapsulated $Gd^{3+}$ cations, disordered over 30 equivalent positions and thereby forming an (underoccupied) icosidodecahedron, is coordinated to a sulfate group that acts as a bidentate ligand to a $\{Mo_2\}$ linker, six water molecules from the encapsulated outer water shell, and two from the inner shell. Each $Gd^{3+}$ ion has a distorted bicapped square prism environment with Gd–O bond lengths in the range of 2.19–2.90 Å (average 2.59 Å). In this sense, the two water shells behave as polydentate/macrocyclic ligands.[3f,3i] The coordination of the $Gd^{3+}$ cations to the sulfate ligands can be seen from the influence of the

  

Table 1. The O···O distances in the water aggregate.

| O···O distances in the $\{H_2O\}_{60+20}$ type aggregate | | | | | |
|---|---|---|---|---|---|
| Atom | Atom | Distance [Å] | Atom | Atom | Distance [Å] |
| O109 | O102 | 1.973 | O105 | O101 | 2.666 |
| O111 | O99 | 2.107 | O102 | O108 | 2.688 |
| O100 | O110 | 2.128 | O104 | O109 | 2.743 |
| O103 | O112 | 2.213 | O102 | O99 | 2.757 |
| O111 | O106 | 2.299 | O104 | O100 | 2.773 |
| O103 | O101 | 2.397 | O108 | O110 | 2.797 |
| O110 | O107 | 2.504 | O108 | O106 | 2.868 |
| O105 | O111 | 2.506 | O105 | O100 | 2.897 |
| O106 | O107 | 2.513 | O103 | O104 | 2.934 |
| O101 | O109 | 2.637 | O107 | O99 | 3.025 |
| O···O distances in the inner small $\{H_2O\}_{20}$ type aggregate | | | | | |
| Atom | Atom | Distance [Å] | Atom | Atom | Distance [Å] |
| O95 | O98 | 3.368 | O96 | O98 | 3.642 |
| O95 | O96 | 3.439 | O95 | O97 | 3.717 |
| O96 | O98 | 3.499 | | | |

cation on the characteristic splitting of the $\nu_{as}(SO_4)$ = $\nu_3(F_2)$ bands (Figure S2).

In addition, the overall anion, with encapsulated $Gd^{3+}$ cations, is categorized as type I within the Robin–Day classification for mixed-valence compounds, which is clearly evident from its UV/Vis spectrum showing a broad band at approximately 460 nm (Figure S3), as well as from the red-brown color of the substance.[3a,4]

The 20 pores of the $\{Mo_9O_9\}$ type are completely closed by the 20 $HC(NH_2)_2^+$ guest cations, which interact through hydrogen bonds with the ring oxygen atoms, demonstrating super-supramolecular chemistry (Figures 1b and 1c). Due to their smaller size and lower affinity to the $\{Mo_9O_9\}$ rings relative to guanidinium cations,[3b] the 20 guest cations are swallowed by the capsule and are located on average approximately 0.4 Å below the centers of the $\{Mo_9O_9\}$ rings. The abundance of the $HC(NH_2)_2^+$ guest cations in **1** is also proven by the appearance of the characteristic IR bands at 1722, 1623, and 1326 $cm^{-1}$ (Figure S2).

The external $Gd^{3+}$ cations and $HC(NH_2)_2^+$ cations cannot be located from single-crystal X-ray diffraction analysis probably due to serious disorder in the crystal lattice, though the elemental analysis and magnetic susceptibility measurement (see below) prove their presence in the crystal.

## Magnetic Properties

Figure 2 shows the product of magnetic susceptibility and temperature ($\chi_M T$) as function of temperature for **1**. The $\chi_M T$ (where $\chi_M$ is the molar magnetic susceptibility) at 290 K has a value of 44.89 $cm^3 K mol^{-1}$, which is close to the spin-only value of 46.77 $cm^3 K mol^{-1}$ (for $g$ = 1.99) and corresponds to the presence of six isolated $Gd^{3+}$ ($^8S_{7/2}$) centers,[5] which is in good agreement with our X-ray crystallographic study and elemental analysis result. The $\chi_M T$ value gradually decreases to 43.79 $cm^3 K mol^{-1}$ on decreasing the temperature to 11 K, it then abruptly reaches the minimum (31.43 $cm^3 K mol^{-1}$) at 2 K. The nature of the plot reveals the presence of very weak antiferromagnetic interactions between the metal centers. The Curie–Weiss fit of the susceptibility data as a function of temperature (Figure S4) gives a Curie constant of 45.00 $cm^3 K mol^{-1}$, which is in excellent agreement with the room-temperature value of $\chi_M T$. The small Weiss temperature of $\theta = 1.0 \pm 0.2$ K shows that the magnetic centers are only very weakly interacting, which is not surprising since there is a large separation between them.

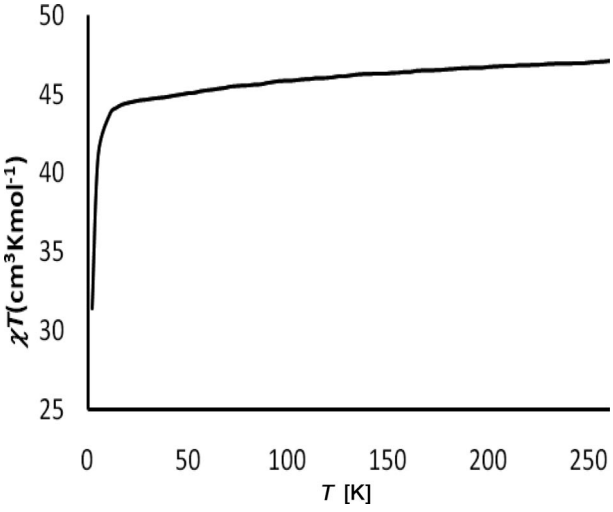


Figure 2. $\chi_M T$ vs. $T$ plot of compound **1**.

## Nonlinear Optical Properties

The nonlinear optical properties of **1** were primarily investigated by single beam Z-scan technology, a well-known and efficient technique for the determination of the nonlinear optical parameters of a material, providing simultaneously the third-order nonlinear susceptibilities, the magnitude of the nonlinear absorption, and the magnitude and sign of the nonlinear refraction of the material under study.[6]

Our Z-scan experiments were performed by using an EKSPLA NL303 Q-switched Nd:YAG laser at 532 nm with a pulse duration of 5 ns and a repetition rate of 10 Hz. The laser beam, after being focused by a 20 cm focal length lens into the sample placed in a quartz cell with a 1 mm path length, was passed through a large-area beam splitter. The transmitted beam was passed through an aperture in the far field and then measured by a photomultiplier. The reflected beam was collected by a large-aperture lens (ensuring collection of the total light transmitted through the sample) and then measured by a photomultiplier. The variation of the transmission of the focused laser beam in these two cases, as a function of the sample distance from the focal plane, gives rise to closed- and open-aperture Z-scan measurements, respectively. The beam waist radius at the focus, $\omega_0$, was determined to be about 16 μm, and the sample position with respect to the focal plane of the laser beam was controlled by a computer-controlled stepper motor.

  

The nonlinear refraction and absorption of the aqueous solution of **1** at a concentration of $1.0\times 10^{-5}$ mol/L was measured by the Z-scan setup described above. From Figure 3, it is known that the depth of peak and the valley are almost symmetrical, which indicates that the nonlinear absorption is weak; this is also confirmed by the open-aperture Z-scan experiment, which shows that the depth of the valley of this curve is so small that it can be ignored.

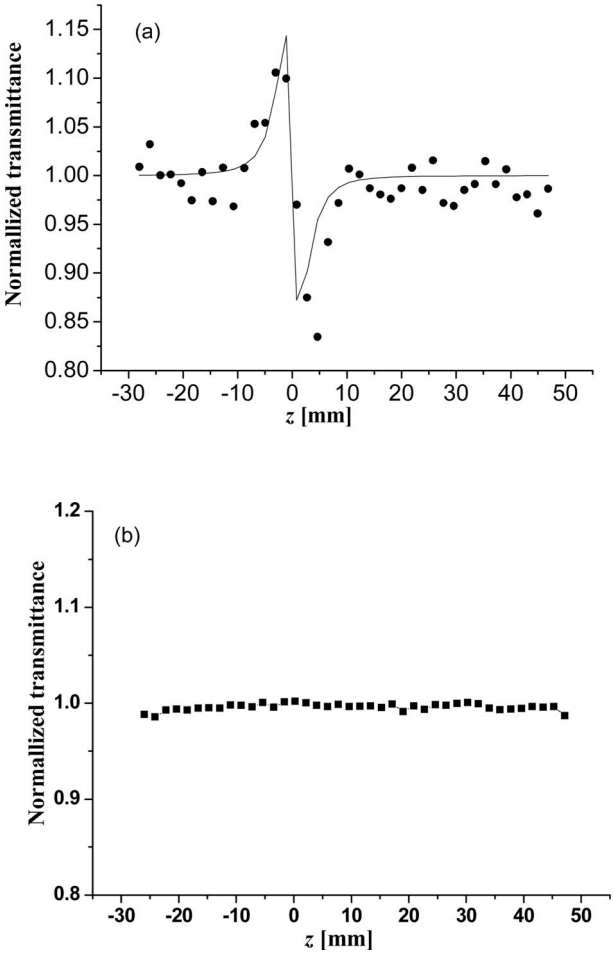


Figure 3. The normalized closed-aperture transmittance curve for compound **1** ($1.0\times 10^{-5}$ mol L$^{-1}$) in water under closed- (a) and open- (b) aperture configurations with 532 nm, 5 ns laser pulses. The optical path is 1 mm. The solid curves are the theoretical fit based on Z-scan theory.

The following formulas are used to calculate the third-order nonlinear refractive index $n_2$ and the real part of the third-order optical nonlinear susceptibility $\chi^{(3)}$ [Equations (1), (2), (3), (4), and (5)].

$$\Delta T_{p-v} = 0.406(1 - s)^{0.25}|\Delta\Phi_0| \quad (1)$$

$$\Delta\Phi_0 = KL_{eff}\,\gamma I_0 \quad (2)$$

$$L_{eff} = (1 - e^{-\alpha_0 L})/\alpha \quad (3)$$

$$n_2\ (esu) = (cn_0/40\pi)\gamma \quad (4)$$

$$Re\chi^{(3)}\ (esu) = (cn_0/160\pi^2)\gamma \quad (5)$$

Where, $\Delta T_{p-v}$ is the difference between the normalized peak and valley transmittance, $s$ is the transmittance of an aperture, $I_0$ is the intensity of the light at focus, $\Delta\Phi_0$ is the phase shift of the beam at the focus, $L_{eff}$ is the effective length of the sample, $\alpha_0$ is the linear absorption coefficient, $\gamma$ is the optical Kerr constant, $L$ is the true optical path length through the sample, $n_0$ is the linear refractive index, $c$ is the speed of light, $n_2$ is the third-order refractive index, and $Re\chi^{(3)}$ is the real part of the third-order optical nonlinear susceptibility.

The parameters $\Delta T_{p-v}$, $s$, $I_0$, $L$, and $\alpha_0$ were measured as 0.28, 0.25, $4.22\times 10^{12}$ W/m$^2$, 1.0 mm, and 221 m$^{-1}$, respectively, and the values of $n_2$ and $\chi^{(3)}$ were subsequently calculated to be $-5.27\times 10^{-11}$ and $-5.76\times 10^{-12}$ esu, respectively. For comparison, the NLO properties of $1.0\times 10^{-5}$ mol L$^{-1}$ aqueous solutions of compound **2** and the parent compound $(NH_4)_{42}[Mo_{132}O_{372}(CH_3COO)_{30}(H_2O)_{72}]$·ca.$300H_2O$·ca.$10CH_3COONH_4$ (**5**),[3a] in which the anions possess similar structures and the cations are simple $NH_4^+$, were also measured by the Z-scan technique under similar experimental conditions at a wavelength of 532 nm with a pulse duration of 5 ns and a repetition rate of 10 Hz. The calculated values of $\chi^{(3)}$ were $-0.85\times 10^{-12}$ for **2** and $-4.21\times 10^{-12}$ esu for **5**, respectively. Interestingly, compounds **1**, **2**, and **5** all show negligible NLO absorption under open-aperture conditions as show in Figure 3b, and the magnitudes of the values of $\chi^{(3)}$ are comparable with each other. However, it is too early to conclude that the role of the water clustering or the presence of the $Gd^{3+}$ and $NH_2CHNH_2^+$ ions has an effect on the NLO properties on the basis of the current data, and we prefer to believe that the NLO properties come from the anion skeleton itself instead of $Gd^{3+}$ and other cations.

The compounds described herein show strong self-defocusing properties under current experimental conditions, which may lead to applications in the protection of optical sensors.

## Conclusions

In summary, we have synthesized and thoroughly characterized a new derivative of the highly charged inorganic super fullerene of the type {pentagon}$_{12}${linker}$_{30}$ ≡ {(Mo)-$Mo_5O_{21}(H_2O)_6$}$_{12}${$Mo_2O_4(SO_4)$}$_{30}$. The internal surface of the capsule is decorated with $Gd^{3+}$ ions coordinated via covalent bonds and, at the outer surface, 20 crown ether type pores are covered by 20 hydrogen-bonded $HC(NH_2)_2^+$ cations, demonstrating a surface supramolecular chemistry. Within the cavity of the capsule a new underoccupied two-shell [$\{H_2O\}_{60+20}$ + $\{H_2O\}_{20}$] water aggregate is located, which acts as a polydentate ligand towards the $Gd^{3+}$ cations. Importantly, the compound shows good self-defocusing third-order nonlinear optical properties. This work has led us to believe that a variety of derivatives of the inorganic super fullerenes with enhanced NLO responses can be synthesized by modification of the electronic structure, which may open new perspectives in the field of functional materials.

  

## Experimental Section

**Materials and Instrumentation:** All reagent grade chemicals and solvents were used as received. IR spectra were recorded with a MAGNA-IR 750 (Nicolet) spectrophotometer by using KBr pellets in the range 400–4000 $cm^{-1}$. Elemental analyses were performed with an Elemental Vario EL III analytical instrument. UV/Vis absorption spectra were recorded with a Shimadzu UV-2550 spectrophotometer. Raman spectra were recorded with a T64000 research Raman spectrometer. Magnetic susceptibility measurements were carried out on a freshly prepared polycrystalline sample with a Quantum Design SQUID magnetometer MPMS-XL. Magnetic measurements of dc type were performed with an applied field of 1 T in the 2–290 K temperature range. Diamagnetic corrections were made from the Pascal constants.[7]

**X-ray Crystallographic Studies:** Single crystals of **1** were removed from the mother liquor and immediately cooled to 113(2) K on a Smart APEX CCD X diffractometer using graphite-monochromatized Mo-$K_\alpha$ radiation ($\lambda$ = 0.71073 Å) and the $\omega$-scan technique. Lorentz polarization and multiscan absorption corrections were applied. The structure was solved by direct methods and refined with full-matrix least-squares techniques using the SHELXS-97 and SHELXL-97 programs.[8] CCDC-763784 contains the supplementary crystallographic data for this paper. These data can be obtained free of charge from The Cambridge Crystallographic Data Centre via www.ccdc.cam.ac.uk/data_request/cif. The details of the X-ray crystallographic data are summarized in Table S1.

**1:** To an aqueous solution (20 mL) of **2** (0.065 mmol, 1.91 g) was added $GdCl_3{\cdot}6H_2O$ (2.64 mmol, 0.98 g) in $H_2O$ (10 mL), and the mixture was stirred for 5 min at room temperature. $NH_2CH(=NH){\cdot}HCl$ (3.01 mmol, 0.24 g) was added to the solution and stirring was continued for an additional 30 min before $H_2SO_4$ (2.5 mL, 2 M) and $NH_4Cl$ (9.51 mmol, 0.51 g) were added. After stirring for a further 30 min, the solution was filtered, and dark brown crystals of **1** precipitated after 1 d. Crystals were collected by filtration, washed with ice-cold water, and dried in air. Yield: 0.4 g, 20% (based on Mo). $C_{26}H_{986}Gd_6Mo_{132}N_{80}O_{864}S_{30}$ (30820.33): calcd. C 1.01, H 3.22, N 3.64, Gd 3.06; found C 1.1, H 2.9, N 3.6, Gd 2.9. Characteristic IR bands (KBr pellet): $\tilde{\nu}$ = 1722 (m), 1623 (m) [$\delta(H_2O)$], 1407 (m–w) [$\delta(NH_4^+)$], 1182 (w), 1134 (m–w), 1064 (w) [$\upsilon_{as}(SO_4)$], 972 (sh, s) [$\upsilon$(Mo=O)], 855 (s), 798 (vs), 726 (vs), 633 (m), 570 (s), 474 $cm^{-1}$. Characteristic Raman bands assignable to the irreducible representations $A_{1g}$ and $H_g$ (solid state, KBr dilution, $\lambda_e$ = 488 nm): $\tilde{\nu}$ = 954 (w), 873 (s), 718 (w), 374 (s), 301 (m–s) $cm^{-1}$. Characteristic UV/Vis band ($H_2O$): $\lambda$ = 460 nm.

**Supporting Information** (see footnote on the first page of this article): Crystallographic data for **1**, Raman and IR spectra of **1** and **2**, UV/Vis spectrum of **1**, and the Curie–Weiss fit of the susceptibility data of **1** as a function of temperature.

## Acknowledgments

The support of the National Natural Science Foundation of China (Grant No. 20541001, 20771012) and the Scientific Research Foundation for the Returned Overseas Chinese Scholars, State Education Ministry (SRF for ROCS, SEM) is gratefully acknowledged. The authors thank Dr. Hartmut Bögge for his kind help in the crystal structure analysis process.

[1] a) G. Maayan, R. Popovitz-Biro, R. Neumann, *J. Am. Chem. Soc.* **2006**, *128*, 4968–4969; b) N. Mizuno, M. Misono, *Chem. Rev.* **1998**, *98*, 199–218; c) J. T. Rhule, C. L. Hill, D. A. Judd, R. F. Schinazi, *Chem. Rev.* **1998**, *98*, 327–357; d) T. Yamase, *Chem. Rev.* **1998**, *98*, 307–325.

[2] a) H. Naruke, T. Ozeki, T. Yamase, *Acta Crystallogr., Sect. C* **1991**, *47*, 489–492; b) A. Müller, E. Krickemeyer, S. Dillinger, J. Meyer, H. Bögge, A. Stammler, *Angew. Chem. Int. Ed. Engl.* **1996**, *35*, 171–173; c) A. Müller, F. Peters, M. T. Pope, D. Gatteschi, *Chem. Rev.* **1998**, *98*, 239–271; d) J. M. Clemente-Juan, E. Coronado, A. Forment-Aliaga, J. R. Galán-Mascarós, S. C. Giménez, C. J. Gómez-García, *Inorg. Chem.* **2004**, *43*, 2689–2694.

[3] a) A. Müller, E. Krickemeyer, H. Bögge, M. Schmidtmann, F. Peters, *Angew. Chem. Int. Ed.* **1998**, *37*, 3360–3363; b) A. Müller, E. Krickemeyer, H. Bögge, M. Schmidtmann, S. Roy, A. Berkle, *Angew. Chem. Int. Ed.* **2002**, *41*, 3604–3609; c) A. Merca, E. T. K. Haupt, T. Mitra, H. Bögge, D. Rehder, A. Müller, *Chem. Eur. J.* **2007**, *13*, 7650–7658; d) A. Müller, S. K. Das, S. Talismanov, S. Roy, E. Beckmann, H. Bögge, M. Schmidtmann, A. Merca, A. Berkle, L. Allouche, Y. Zhou, L. Zhang, *Angew. Chem. Int. Ed.* **2003**, *42*, 5039–5044; e) A. Müller, E. Krickemeyer, H. Bögge, M. Schmidtmann, B. Botar, M. O. Talismanova, *Angew. Chem. Int. Ed.* **2003**, *42*, 2085–2090; f) A. Müller, Y. Zhou, L. Zhang, H. Bögge, M. Schmidtmann, M. Dressel, J. van Slageren, *Chem. Commun.* **2004**, 2038–2039; g) A. Ziv, A. Grego, S. Kopilevich, L. Zeiri, P. Miro, C. Bo, A. Müller, I. A. Weinstock, *J. Am. Chem. Soc.* **2009**, *131*, 6380–6382; h) C. Schäffer, H. Bögge, A. Merca, I. A. Weinstock, D. Rehder, E. T. K. Haupt, A. Müller, *Angew. Chem. Int. Ed.* **2009**, *48*, 8051–8056; i) A. Müller, Y. Zhou, H. Bögge, M. Schmidtmann, T. Mitra, E. T. K. Haupt, A. Berkle, *Angew. Chem. Int. Ed.* **2006**, *45*, 460–465; j) A. Müller, *Nature* **2007**, *447*, 1035, and references cited therein.

[4] M. B. Robin, P. Day, *Adv. Inorg. Chem. Radiochem.* **1967**, *10*, 247–422.

[5] a) C. Benelli, D. Gatteschi, *Chem. Rev.* **2002**, *102*, 2369–2387; b) W. P. W. Lai, W. T. Wong, B. K. F. Li, K. W. Cheah, *New J. Chem.* **2002**, *26*, 576–581.

[6] M. Sheik-Bahae, A. A. Said, T.-H. Wei, D. J. Hangan, E. W. Van Stryland, *IEEE J. Quantum Electron.* **1990**, *26*, 760–769.

[7] O. Kahn, *Molecular Magnetism*, VCH Publishers, New York, **1993**.

[8] G. M. Sheldrick, *SHELXL97 and SHELXS97*, *Program for X-ray Crystal Structure Solution and Refinement*, University of Göttingen, Göttingen, Germany, **1997**.

Received: January 29, 2010
Published Online: May 7, 2010

  